

# A catalogue of absorption lines in eight *Hubble Space Telescope*/STIS E230M $1.0 < z < 1.7$ quasar spectra<sup>★</sup>

N. Milutinović,<sup>1,2†</sup> T. Misawa,<sup>1†</sup> R. S. Lynch,<sup>1,3†</sup> J. R. Masiero,<sup>1,4†</sup> C. Palma,<sup>1†</sup>  
J. C. Charlton,<sup>1†</sup> D. Kirkman,<sup>5†</sup> S. Bockenhauer<sup>5†</sup> and D. Tytler<sup>5†</sup>

<sup>1</sup>Department of Astronomy & Astrophysics, 525 Davey Lab, Pennsylvania State University, University Park, PA 16802, USA

<sup>2</sup>Department of Physics & Astronomy, University of Victoria, Elliott Building, 3800 Finnerty Road, Victoria, BC, Canada V8P 5C2

<sup>3</sup>Department of Astronomy, PO Box 400325, University of Virginia, Charlottesville, VA 22904, USA

<sup>4</sup>Institute for Astronomy, University of Hawaii, 2680 Woodlawn Drive, Honolulu, HI 96822, USA

<sup>5</sup>Center for Astrophysics and Space Sciences, University of California, San Diego, MS 0424, La Jolla, CA 92093-0424, USA

Accepted 2007 June 7. Received 2007 June 7; in original form 2007 April 27

## ABSTRACT

We have produced a catalogue of line identifications and equivalent width measurements for all absorption features in eight ultraviolet echelle quasar spectra. These spectra were selected as having the highest signal-to-noise ratio among the *Hubble Space Telescope*/STIS spectra obtained with the E230M grating. We identify 56 metal-line systems towards the eight quasars, and present plots of detected transitions, aligned in velocity space. We found that about 1/4–1/3 of the features in the Ly $\alpha$  forest region, redward of the incidence of the Ly $\beta$  forest, are metal lines. High-ionization transitions are common. At the redshift range we study,  $z < 1.7$ , we see both O VI and C IV in 88–90 per cent of the metal-line systems for which the spectra cover the expected wavelength. Si III is seen in 58 per cent, while low-ionization absorption in C II, Si II and/or Al II is detected in 50 per cent of the systems for which they are covered. This catalogue will facilitate future studies of the Ly $\alpha$  forest and of metal-line systems of various types.

**Key words:** intergalactic medium – quasars: absorption lines.

## 1 INTRODUCTION

The most important chemical transitions for quasar absorption-line systems at low redshift (e.g.  $z < 1$ ) still lay in the ultraviolet (UV) spectral range. A limited number of the most UV-bright quasars have been observed with the *Hubble Space Telescope* (*HST*)/Space Telescope Imaging Spectrograph (STIS), which has provided a detailed view of absorption systems along the lines of sight. These data are available from the Multimission Archive at Space Telescope. However, in order to compile statistics of absorbers or to study particular systems, it is necessary to identify the spectral features. This can be complicated, particularly in the Ly $\alpha$  forest region, and when the available spectral coverage is limited.

In the course of our studies of the Ly $\alpha$  forest and metal-line systems we have studied in detail eight of the highest quality *HST*/STIS spectra, obtained with the E230M grating. In this paper we present

these spectra with a list of  $5\sigma$  absorption features and our suggested line identifications. In particular, metal-line system identifications are necessary in order to remove contaminants from the Ly $\alpha$  forest. In a recent paper (Kirkman et al. 2007), we measured statistics of absorption in the Ly $\alpha$  forest at  $0 < z < 1.6$  using 74 low-resolution *HST*/FOS quasar spectra. As a check, and particularly to assess our ability to separate metal lines from the forest, we also used the available higher resolution E230M *HST*/STIS spectra. In the present paper, we present the relevant data and line identifications which were used in that paper. We expect that this catalogue will facilitate future studies of metal-line absorption systems as well as of the Ly $\alpha$  forest.

Our catalogue includes damped Ly $\alpha$  absorbers (DLAs), Lyman limit systems and Ly $\alpha$  forest clouds. The DLA and Lyman limit systems are expected to have strong Mg II absorption (Churchill et al. 2000; Rao & Turnshek 2000), while the Ly $\alpha$  forest clouds may have weak Mg II and other low-ionization transitions detected (such as Si II and C II) (Narayanan et al. 2005). Some Ly $\alpha$  forest clouds have detected C IV and/or O VI, without associated low-ionization absorption (Tripp, Savage & Jenkins 2000; Savage et al. 2002; Milutinović et al. 2006). The catalogue that we will present will allow for future studies of the various types of absorbers.

In Section 2 we describe *HST*/STIS quasar spectra and our reduction and continuum fitting procedures. We also outline our line detection and measurement algorithms and line identification

<sup>★</sup>Based on observations obtained with the NASA/ESA *Hubble Space Telescope*, which is operated by the Space Telescope Science Institute (STScI) for the Association of Universities for Research in Astronomy, Inc., under NASA contract NAS5D26555.

†E-mail: milni@uvic.ca (NM); misawa@astro.psu.edu (TM); rsl4v@virginia.edu (RSL); masiero@ifa.hawaii.edu (JRM); cpalma@astro.psu.edu (CP); charlton@astro.psu.edu (JCC); dkirkman@ucsd.edu (DK); sbockenhauer@wisc.edu (SB); tytler@ucsd.edu (DT)

**Table 1.** *HST*/STIS E230M quasar observations.

QSO ID	$z_{\text{em}}$	S/N <sup>a</sup>		PI	Proposal ID	$\lambda_{\text{lo}}$ (Å)	$\lambda_{\text{up}}$ (Å)	$N_{\text{tot}}^b$	$N_{\text{metal}}^c$	$N_{\text{Gal}}^d$
		2382 Å	2796 Å							
PG 0117+210	1.491	8.5	14.2	Jannuzi	8673	2278.7	3117.0	104	31	10
HE 0515–4414	1.713	8.1	22.0	Reimers	8288	2274.8	3118.9	63	13	9
PG 1206+459	1.160	8.4	15.4	Churchill	8672	2277.1	3116.4	85	33	9
PG 1241+176	1.273	5.2	20.0	Churchill	8672	2276.9	3066.0	62	20	10
PG 1248+401	1.030	8.1	9.6	Churchill	8672	2276.7	3107.7	41	14	10
CSO 873 <sup>e</sup>	1.022	8.0	10.4	Churchill	8672	2278.4	3119.2	26	3	8
PG 1634+706	1.334	19.8	28.5	Jannuzi/Burles	8312/7292	1860.7	3117.0	121	33	18
PG 1718+481	1.083	15.9	...	Burles	7292	1848.4	2672.7	81	15	14

<sup>a</sup>S/N per pixel at 2382 Å and 2796 Å; <sup>b</sup>total number of absorption features between Ly $\alpha$  and Ly $\beta$  emission lines of quasar; <sup>c</sup>number of identified metal absorption features between Ly $\alpha$  and Ly $\beta$  emission lines of quasar; <sup>d</sup>number of Galactic metal absorption features in entire observed wavelength region; <sup>e</sup>coordinate of this quasar: RA 13<sup>h</sup>19<sup>m</sup>56<sup>s</sup>.3, Dec. +27°28′09″ (J2000.0).

strategies. The normalized echelle spectra are presented in Section 3, along with a brief description of metal-line systems detected towards each quasar. System plots, showing all detected transitions for each system, are also presented there. In Section 4 we present a general summary of the systems presented in this catalogue.

## 2 DATA AND METHODS

We selected the eight  $z > 1$  quasars observed with the *HST*/STIS E230M grating which had a signal-to-noise ratio, S/N > 5, over a reasonable fraction of the spectrum. These *HST*/STIS E230M spectra have a resolution  $R = 30\,000$ , with two pixels per resolution element. Our sample is biased towards quasars that have Lyman limit systems, since most of the STIS observations were conducted in order to study those particular known systems in detail.

Several settings are possible covering different wavelength ranges. For seven of the eight quasars in our sample, 2280–3110 Å is covered. The quasars and the relevant observational details are listed in Table 1. Specifically, this table lists quasar redshifts, wavelength coverage, S/N per pixel at 2350 and 2750 Å, primary investigator for the original observation, and proposal ID.

The data were reduced using the STIS pipeline (Brown et al. 2002). They were combined by simple weighting by exposure time (as in Narayanan et al. 2005), rather than by, for example, inverse variance methods that are often employed. A bias could be introduced by the latter method, since pixels with smaller counts would be weighted more heavily. This bias is significant only in cases such as these STIS spectra, where individual exposures have very small S/N, and is not typically important for reduction of ground-based high-resolution echelle spectra.

Wavelengths were corrected to the heliocentric reference frame. When the same quasar was observed multiple times, there was often a small shift in wavelength between the spectra, due to the intentional shifting of the echelle angle of the instrument. In this case, we chose not to smooth the data by interpolating, but instead chose wavelength bins from one exposure and combined the flux from other exposures into the nearest bin. This results in a slightly decreased effective resolution. Continuum fits used the standard IRAF SFIT task.<sup>1</sup>

Features were objectively identified by searching for an unresolved line at each pixel (as employed in Schneider et al. 1993),

and applying a  $5\sigma$  criterion for detection. However, we found by inspection that some of these formal detections are not likely to be real. In some cases, only 1 pixel had significant absorption, and in other cases it appeared that correlated noise biased the measurement. Features that are broad and shallow can be  $>5\sigma$  and yet look unconvincing because they are sensitive to the continuum level. Such spurious features, estimated to be 10 per cent of the total number of detections, were eliminated from consideration. We define a feature as all the pixels around a  $5\sigma$  detection that have not recover to the continuum after smoothing the spectra using an equation on p. 56 of Schneider et al. (1993). This definition means that many features are clear blends of well-separated lines; and hence a feature can have more than one identification, each of which may be secure because they refer to different blended lines. Wavelength that we give for a feature is the flux-weighted central value, the mean of the wavelengths where the smoothed flux drops below the continuum, with weighting for the fraction of the photons that are absorbed at each pixel. If metal lines blend with other non-related absorption profiles severely, we manually select spectral regions over which the flux-weighted central wavelength is calculated.

We attempted to identify all features in each of the quasar spectrum, and the transitions that were identified one or more times are listed with their vacuum wavelengths and oscillator strengths in Table 2. For our line identification we used the following procedure.

(i) Examine the spectrum at the expected positions of possible Galactic lines, and mark all possible detections.

(ii) Search for the strong resonant doublet transitions: Mg II  $\lambda\lambda$ 2796, 2803, Si IV  $\lambda\lambda$ 1394, 1403, C IV  $\lambda\lambda$ 1548, 1551, N V  $\lambda\lambda$ 1239, 1243 and O VI  $\lambda$   $\lambda$ 1032, 1038. In addition to these, we also search for low-ionization gas through the combination C II  $\lambda$ 1335 and Si II  $\lambda$ 1260, which can be used in place of Mg II  $\lambda\lambda$  2796, 2803 when the latter is not covered (Narayanan et al. 2005; Milutinović et al. 2006).

(iii) Check positions of other transitions that could be detected for systems found through the doublet search, including the Lyman series lines. If a system is ambiguous with the doublet alone, Ly $\alpha$  and other Lyman series lines were used to assess its reality.

(iv) Having completed these steps, all features that remain without plausible identifications are considered to be Lyman series lines.

(v) Begin by assuming that the highest order Lyman series line is the correct identification and search for all of the stronger (lower order) Lyman series lines corresponding to the same redshift. If reasonable ratios are found, mark these as possible identifications.

<sup>1</sup> IRAF is distributed by the National Optical Astronomy Observatories, which are operated by AURA, Inc., under contract to the National Science Foundation.

**Table 2.** Detected transitions.

Transition	$\lambda_{\text{rest}}^a$ (Å)	Oscillator strength <sup>a</sup>
Ly $\alpha$	1215.6701	0.416 400
H I $\lambda$ 1026	1025.7223	0.079 120
H I $\lambda$ 972	972.5368	0.029 000
H I $\lambda$ 950	949.7431	0.013 940
H I $\lambda$ 938	937.8035	0.007 799
H I $\lambda$ 931	930.7483	0.004 814
H I $\lambda$ 926	926.2257	0.003 183
H I $\lambda$ 923	923.1504	0.002 216
H I $\lambda$ 921	920.9631	0.001 605
H I $\lambda$ 919	919.3514	0.001 20
C I $\lambda$ 1158	1157.910	0.021 780
C I $\lambda$ 1189	1188.833	0.016 760
C I $\lambda$ 1277	1277.245	0.096 650
C I $\lambda$ 1329	1328.833	0.058 040
C II $\lambda$ 1036	1036.3367	0.1231
C II $\lambda$ 1335	1335.31	0.127
C II * $\lambda$ 1336b	1335.6627	0.012 77
C III $\lambda$ 977	977.020	0.7620
C IV $\lambda$ 1548	1548.195	0.190 800
C IV $\lambda$ 1551	1550.770	0.095 220
N I $\lambda$ 1134b	1134.1653	0.013 42
N I $\lambda$ 1135	1134.9803	0.040 23
N I $\lambda$ 1201	1200.7098	0.044 23
N II $\lambda$ 1084	1083.990	0.1031
N V $\lambda$ 1239	1238.821	0.157 000
N V $\lambda$ 1243	1242.804	0.078 230
O VI $\lambda$ 1032	1031.927	0.132 900
O VI $\lambda$ 1038	1037.616	0.066 090
Mg I $\lambda$ 2853	2852.964	1.810 000
Mg II $\lambda$ 2796	2796.352	0.6123
Mg II $\lambda$ 2803	2803.531	0.3054
Al II $\lambda$ 1671	1670.787	1.880 000
Al III $\lambda$ 1855	1854.716	0.539 000
Si II $\lambda$ 990	989.873	0.133 000
Si II $\lambda$ 1190	1190.416	0.250 200
Si II $\lambda$ 1193	1193.290	0.499 100
Si II * $\lambda$ 1195	1194.500	0.623 300
Si II $\lambda$ 1260	1260.422	1.007 000
Si II $\lambda$ 1304	1304.370	0.147 300
Si II $\lambda$ 1527	1526.707	0.116 00
Si III $\lambda$ 1207	1206.500	1.660 000
Si IV $\lambda$ 1394	1393.755	0.528 000
Si IV $\lambda$ 1403	1402.770	0.262 000
P II $\lambda$ 1153	1152.818	0.236 100
S II $\lambda$ 1251	1250.584	0.005 453
Cr II $\lambda$ 2056	2056.254	0.1403
Cr II $\lambda$ 2062	2062.234	0.1049
Cr II $\lambda$ 2066	2066.161	0.069 82
Mn II $\lambda$ 2577	2576.877	0.3508
Mn II $\lambda$ 2594	2594.499	0.2710
Mn II $\lambda$ 2606	2606.461	0.1927
Fe I $\lambda$ 2524	2523.608	0.279 000
Fe II $\lambda$ 1608	1608.4449	0.055 450
Fe II $\lambda$ 2250	2249.8768	0.001 82
Fe II $\lambda$ 2261	2260.7805	0.002 44
Fe II $\lambda$ 2344	2344.214	0.109 700
Fe II $\lambda$ 2374	2374.4612	0.028 18
Fe II $\lambda$ 2383	2382.765	0.3006
Fe II $\lambda$ 2587	2586.650	0.064 570
Fe II $\lambda$ 2600	2600.1729	0.223 90
Zn II $\lambda$ 2063	2062.664	0.252 900

<sup>a</sup>These numbers are from Verner, Verner & Ferland (1996).

Otherwise continue assessing the possible identifications of the feature in question until reaching Ly $\alpha$ .

(vi) If no identification, including a Ly $\alpha$  identification, is plausible the feature is left unidentified.

(vii) If more than one identification is reasonable (or if there is likely to be a blend for which more than one system contributes significantly), this is noted.

### 3 RESULTS

Fig. 1 is a sample of a portion of the normalized spectrum of PG 0117+213, shown in the printed version. We present all normalized quasar spectra in Figs 1–8, which are available online; see the Supplementary Material section. Similarly, our listings of line identifications are presented electronically in Table 3, with some sample listings appearing in the printed version. In this table, quasars are ordered by right ascension and  $5\sigma$  features by increasing wavelength within a given quasar entry. In Table 3 we list, for each  $5\sigma$  feature that we did not reject as unconvincing, the observed vacuum wavelength ( $\lambda_{\text{obs}}$ ), the observed frame equivalent width and error [ $W_{\text{obs}}$  and  $\sigma(W_{\text{obs}})$ ] and the significance level ( $S$ ; observed equivalent width/error in equivalent width). It also gives our favoured line identification for each feature (transition and redshift) along with notes that indicate alternative and/or additional identifications. If the identification cannot be confirmed with another line, or is uncertain for some other reason, a ‘?’ is listed after the preferred transition ID. We do not give column densities since there are best done on a system-by-system basis using velocity plots to ensure that the columns for different ions are representative of the same gas.

The following subsections present the eight quasars along with discussion of noteworthy metal-line systems found in their spectra. Fig. 9 presents an illustrative ‘system plot’ for the  $z = 0.5764$  system towards PG 0117+213. The transitions detected at  $5\sigma$  for all of the metal-line systems are plotted in velocity space in the online versions of Figs 9–64 (see the Supplementary Material section). The quasar emission redshifts, taken from the NASA/IPAC Extragalactic Database, are listed in the heading of each subsection.

#### 3.1 PG 0117+213 ( $z_{\text{em}} = 1.493$ )

This quasar was studied as part of the Quasar Absorption Line Key Project, using G270H grating of *HST*/Faint Object Spectrograph (FOS), with resolution of  $R = 1300$ . Jannuzi et al. (1998) found possible metal-line systems at  $z = 0.5766, 0.9400, 0.9676, 1.0724, 1.3389, 1.3426$  and  $1.3868$ . They also found tentative suggestions of metal-line systems at  $z = 1.3256$  and  $1.4952$ . Mg II is detected in a Keck/HIRES spectrum at  $z = 0.5764, 0.7290, 1.0480, 1.3250$  and  $1.3430$  (Churchill et al. 1999; Churchill & Vogt 2001), and these five systems were modelled (including constraints from this STIS coverage) by Masiero et al. (2005).

Jannuzi et al. (1998) observed this quasar with *HST*/STIS to facilitate a statistical study of the Ly $\alpha$  forest. This spectrum covers the Ly $\alpha$  forest over almost all of its wavelength coverage, blueward of 3031 Å. The Ly $\beta$  line is covered blueward of 2558 Å, Ly $\gamma$  blueward of 2423 Å, and Ly $\delta$  blueward of 2368 Å. There is also limited redshift coverage of higher order Lyman series lines. Along this line of sight are five Mg II absorbers. One of them is a DLA, two are strong Mg II absorbers, and the other two are multiple-cloud, weak Mg II absorbers. Three certain, and two possible O VI systems are also detected. The metal-line systems towards this quasar are plotted in Figs 9–18.

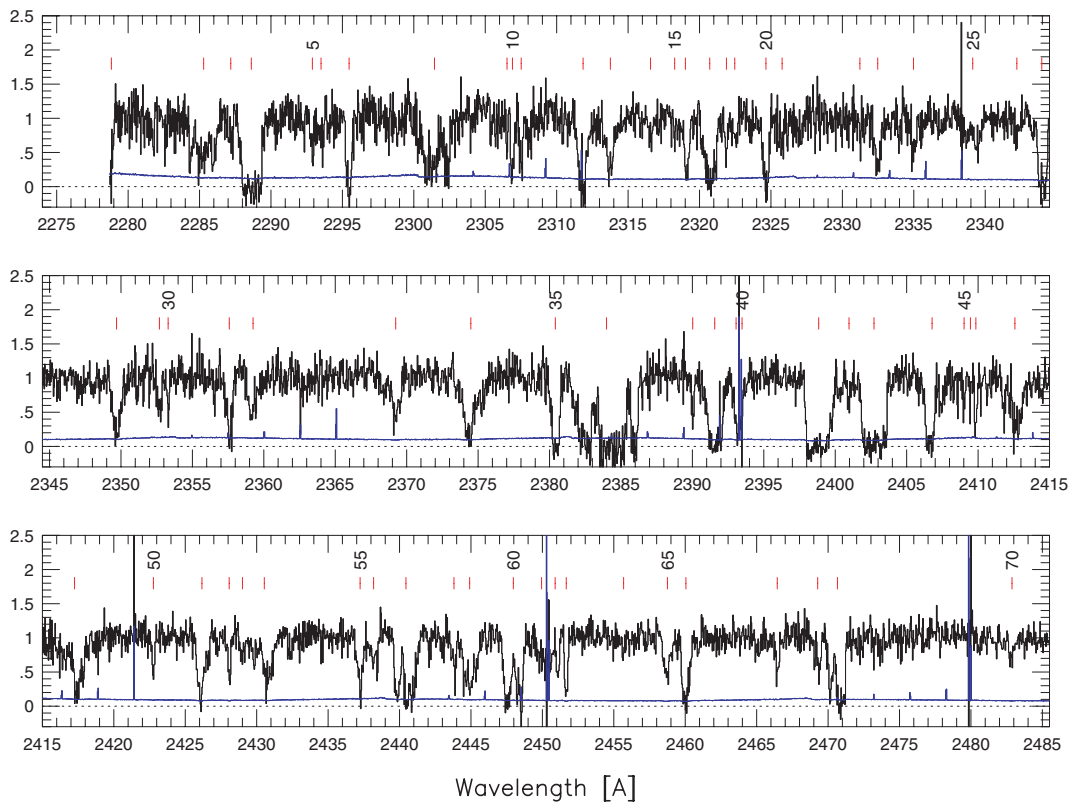


**Figure 1.** Sample – Normalized flux versus wavelength for a portion of the *HST*/E230M spectrum of quasar PG 0117+213. This is an example of a set of figures for all quasars and all wavelength coverage, which are given in the electronic version (see the Supplementary Material section). The histogram displayed beneath the data represents the error spectrum. For reference, a dotted line is drawn at zero flux. Numbered ticks mark spectral features detected at a  $5\sigma$  level. These are listed in Table 3.

$z = 0.5764$ . The  $z = 0.5764$  system is a strong Mg II absorber. Based upon only a low-resolution *HST*/FOS spectrum, obtained in spectropolarimetry mode (Koratkar et al. 1998), it is not clear whether this is a DLA or whether it has multiple undamped components (Rao & Turnshek 2000). In the *HST*/STIS spectrum, C IV  $\lambda\lambda 1548, 1551$  are detected, but both transitions suffer from blending. The C IV  $\lambda 1548$  is blended in its blue component with Ly $\gamma$  from a system at  $z = 1.5088$ . An unidentified blend appears on the red wing of C IV  $\lambda 1550$  and its blueward component also has a small contribution from Si II  $\lambda 1193$  at  $z = 1.0480$ . Al III  $\lambda\lambda 1855, 1863$  is detected, but the blueward member has a blend to its blue, probably with Ly $\alpha$ . Strong Al II  $\lambda 1671$  is detected, as is Fe II  $\lambda 1608$ . The strong feature redward of Al II  $\lambda 1671$  is probably Ly $\alpha$  at  $z = 1.1671$ . In addition to Mg II and Mg I, Ca II and Ti II were detected in the Keck/HIRES spectrum (Masiero et al. 2005).

$z = 0.7290$ . The unusual multiple-cloud, weak Mg II absorber at  $z = 0.7290$  is detected only in Al II  $\lambda 1671$  and C II  $\lambda 1335$  in the *HST*/STIS spectrum. C IV  $\lambda\lambda 1548, 1551$  is covered at a high sensitivity, yet it is not detected to a  $3\sigma$  rest-frame equivalent width limit of  $0.01 \text{ \AA}$ . This makes it ‘C IV-deficient’, possibly indicative of a low level of star formation so that a corona would be weak or absent in its very red, barred spiral galaxy host (Masiero et al. 2005).

$z = 1.0480$ . The  $z = 1.0480$  system was found not to have metal lines detected in the low-resolution *HST*/FOS spectrum. The detections of Si II, C II, Si III, Si IV  $\lambda\lambda 1394, 1403$  in the *HST*/STIS spectrum are consistent with those limits. Unfortunately, the STIS spectrum does not cover C IV  $\lambda\lambda 1548, 1551$ , which would provide useful constraints on the system’s physical conditions. Based upon photoionization modelling (Masiero et al. 2005) it would appear that

there is a significant blend with Si III  $\lambda 1207$ , which is most likely Ly $\alpha$ .

$z = 1.3250$ . The  $z = 1.3250$  system is just above the borderline to qualify as a strong Mg II absorber. It has six weak components in Mg II  $\lambda\lambda 2796, 2803$  spread over  $\sim 250 \text{ km s}^{-1}$  (Churchill & Vogt 2001). There is a partial Lyman limit system detected in an *HST*/FOS spectrum (Jannuzi et al. 1998). In the *HST*/STIS spectrum Si II and C II are detected from the strongest four of these six components. Si III  $\lambda 1207$  is also detected over the full velocity range, but it suffers from a blend with Galactic Mg II  $\lambda 2803$  to the blue. There may also be blends redward of this, based upon the photoionization models (Masiero et al. 2005), but we were unable to provide identifications besides possible Ly $\alpha$ . Unfortunately, C IV  $\lambda\lambda 1548, 1551$ , which was detected in the *HST*/FOS spectrum (Jannuzi et al. 1998), is not covered in the STIS spectrum. There is a possible weak detection of N V  $\lambda 1239$  but it cannot be confirmed using N V  $\lambda 1243$  because it is in a noisy part of the spectrum. A strong O VI  $\lambda\lambda 1032, 1038$  is detected, but O VI  $\lambda 1032$  is blended to the red with Ly $\beta$  from the system at  $z = 1.3390$ , and to the blue with possible Ly $\alpha$ . Also, O VI  $\lambda 1038$  must have a blend, at least on the red wing of its strong component, since that profile is too strong relative to O VI  $\lambda 1032$  at that velocity. This blend could be O VI  $\lambda 1032$  from the  $z = 1.3390$  system. If so, these systems would be ‘line-locked’.

$z = 1.3390$ . We find the evidence for metal lines in the  $z = 1.3390$  system to be inconclusive. Ly $\alpha$  is not detected in the redward portion range of the possible C III  $\lambda 977$  feature, so not all of that absorption can be C III at this redshift. Two components of Si III  $\lambda 1207$  are possible, but they do not align perfectly with the minima of the C III profile and cannot be confirmed in any other way. Also, O VI

**Table 3.** Sample – features with  $5\sigma$  identified in the *HST/STIS* E230M spectra of eight quasars. The full version is available online (see the Supplementary Material section).

#	$\lambda_{\text{obs}}$	$W_{\text{obs}}$	$\sigma(W_{\text{obs}})$	$S$	Line ID PG 0117 + 213 ( $z_{\text{em}} = 1.493$ )	$z$	Notes
1	2278.83	0.21	0.02	9.5	H $\text{I}\lambda 972$	1.3430	
2	2285.29	0.97	0.04	25.7	C $\text{III}\lambda 977$	1.3390	
3	2287.19	0.11	0.02	6.3	Ly $\alpha$ ?	0.8814	
4	2288.62	1.62	0.03	49.4	C $\text{III}\lambda 977$	1.3430	Probable blend with Ly $\alpha$ at $z=0.8026$ ?
5	2292.90	0.14	0.02	7.9	Ly $\alpha$ ?	0.8861	
6	2293.51	0.14	0.02	6.8	Ly $\alpha$ ?	0.8866	
7	2295.47	0.47	0.02	21.4	H $\text{I}\lambda 938$	1.4478	
8	2301.45	1.31	0.05	28.4	Ly $\alpha$ ?	0.8932	Reddest component is H $\text{I}\lambda 950$ at $z = 1.4242$
9	2306.53	0.05	0.01	4.2	Ly $\alpha$ ?	0.8973	
10	2306.91	0.20	0.01	13.9	C $\text{II}\lambda 1335$	0.7290	
11	2307.52	0.18	0.02	11.8	C $\text{II}\lambda 1335$	0.7290	
12	2311.85	0.76	0.04	21.2	H $\text{I}\lambda 1026$	1.2543	
13	2313.76	0.51	0.02	20.9	Ly $\alpha$ ?	0.9033	
14	2316.57	0.09	0.01	6.0	Ly $\alpha$ ?	0.9056	
15	2318.26	0.04	0.01	5.5	Ly $\alpha$ ?	0.9070	Small contribution from N $\text{III}\lambda 989$ at $z = 1.3430$
16	2319.01	0.38	0.02	17.5	Ly $\alpha$ ?	0.9076	
17	2320.72	0.83	0.03	33.0	H $\text{I}\lambda 972$	1.3866	
18	2321.88	0.11	0.01	9.3	H $\text{I}\lambda 931$	1.4949	
19	2322.47	0.13	0.02	6.9	Ly $\alpha$ ?	0.9104	
20	2324.65	0.46	0.02	21.8	H $\text{I}\lambda 950$	1.4478	
21	2325.78	0.06	0.01	5.5	Ly $\alpha$ ?	0.9132	
22	2331.23	0.04	0.01	3.0	H $\text{I}\lambda 972$	1.3983	
23	2332.47	0.37	0.02	16.4	H $\text{I}\lambda 972$	1.3983	
24	2334.98	0.19	0.02	10.1	Ly $\alpha$ ?	0.9207	
25	2339.13	0.40	0.03	12.7	H $\text{I}\lambda 938$	1.4949	
26	2342.22	0.08	0.01	5.5	Ly $\alpha$ ?	0.9267	
27	2343.96	0.77	0.02	35.2	Fe $\text{II}\lambda 2344$	0	
28	2349.69	0.53	0.02	24.8	Fe $\text{II}\lambda 2374$	0	
29	2352.69	0.14	0.02	9.0	Ly $\alpha$ ?	0.9353	
30	2353.30	0.08	0.02	5.2	H $\text{I}\lambda 972$	1.4242	
31	2357.58	0.38	0.02	16.9	Ly $\alpha$ ?	0.9393	
32	2359.25	0.34	0.03	13.5	Ly $\alpha$ ?	0.9407	
33	2369.23	0.35	0.02	18.1	H $\text{I}\lambda 950$	1.4949	Blend to the red with C $\text{III}\lambda 977$ at $z=1.4242$
34	2374.49	0.99	0.03	31.7	Fe $\text{II}\lambda 2374$	0	
35	2380.41	0.66	0.02	27.7	H $\text{I}\lambda 972$	1.4478	

$\lambda\lambda$  1032, 1038 may be detected. The alignment is reasonably good, though the feature redward of the O VI  $\lambda$ 1032 component is likely to be O VI  $\lambda$ 1038 from the system at  $z = 1.3250$ .

$z = 1.3430$ . The  $z = 1.3430$  system is also just at the border between strong and multiple-cloud weak Mg II absorption. Like the  $z = 1.3250$  system, it has a partial Lyman limit break in the *HST/FOS* spectrum (Jannuzi et al. 1998). Ly $\alpha$  and Ly $\beta$  are detected in the *HST/STIS* spectrum along with C II, Si II, N II, C III. There is a feature at the expected position of N III  $\lambda$ 998, which appears to be too strong relative to the other transitions in this system (Masiero et al. 2005). We believe this feature could be Ly $\alpha$  at  $z = 0.9076$ . C IV is not covered in the STIS spectrum, but strong C IV absorption is detected in the FOS spectrum. N V  $\lambda\lambda$ 1239, 1243 appears to be detected, but the N V  $\lambda$ 1239 transition is blended, probably with Ly $\alpha$  at  $z = 1.3866$ .

$z = 1.4242$ . There is an O VI system, with detected Ly $\alpha$ , Ly $\beta$  and Ly $\gamma$  at  $z = 1.4242$ .

$z = 1.4463$ . Another weak, broad O VI doublet at  $z = 1.4463$  is also detected in C III and Si III, as well as in Ly $\alpha$ . The feature in the Si III  $\lambda$ 1207 panel, at  $\sim 40 \text{ km s}^{-1}$ , is at least partially Si II  $\lambda$ 1260 at  $z = 1.3430$  (as is the stronger feature to its red).

$z = 1.4478$ . At  $z = 1.4478$  the Lyman series is detected down to Ly $\epsilon$ , which is the last member covered in the *HST/STIS* spectrum.

There is a possible O VI doublet at this redshift, but the feature at the position of O VI  $\lambda$ 1032 transition does not match the profile of that at the position of O VI  $\lambda$ 1038.

$z = 1.5088$ . The O VI system at  $z = 1.5088$  is another example of associated O VI absorption that appears slightly redward of the quasar emission redshift. It is detected in Ly $\alpha$  and Ly $\beta$ . The Ly $\beta$  shows the same components as O VI, but clearly has a blend to the red, probably with Ly $\alpha$ . Ly $\gamma$  is heavily blended with C IV  $\lambda$ 1548 from the  $z = 0.5764$  system. C III  $\lambda$ 977 is also detected in three components, though the blueward one is affected by a data defect.

### 3.2 HE 0515–4414 ( $z_{\text{em}} = 1.713$ )

This quasar was observed with *HST/STIS* by Reimers et al. (2003) in order to study a sub-DLA at  $z = 1.15$ , for which they also have optical coverage. Their study of this system, particularly focused on molecular hydrogen, is published as Reimers et al. (2003). In addition, Reimers et al. (2003) and Levshakov et al. (2003) report on six O VI systems along the line of sight (at  $z = 1.385$ , 1.416, 1.602, 1.674 and 1.697), based upon the *HST/STIS* spectrum in conjunction with VLT/UVES data. Ly $\alpha$  is covered over the entire *HST/STIS* spectrum, Ly $\beta$  up to 2784 Å, and Ly $\gamma$  is covered up to

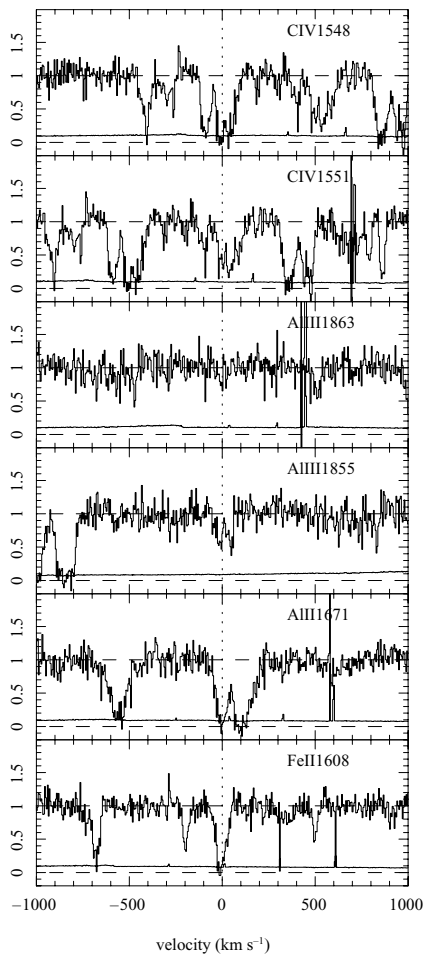


**Figure 9.** Sample – system plot for the  $z = 0.5764$  system towards PG 0117+213. The full version is available online (see the Supplementary Material section). Important transitions are plotted, unless they are so badly compromised by a blend that no useful constraints can be gathered. The transitions are aligned in velocity space, with  $0 \text{ km s}^{-1}$  corresponding to  $z = 0.5764$ . The error spectrum is plotted beneath the data, and a dashed line shown at zero flux.

2651 Å. There is more limited coverage of all other Lyman series transitions down to the Lyman limit of the quasar.

The *HST*/*STIS* spectrum is dominated by the sub-DLA at  $z = 1.15$  and its many detected metal and molecular hydrogen transitions. In addition, there is one C IV system, four definite O VI systems, and three possible O VI systems. A couple of these O VI systems are associated. System plots for this quasar are given in Figs 19–27.

$z = 0.9406$ . A two-component C IV doublet is detected at  $z = 0.9406$ , which also has Ly $\alpha$  and Si III detected. Si IV is also probably detected in the redward component, but this cannot be confirmed because Si IV  $\lambda 1394$  is blended with an unknown line, probably Ly $\alpha$ .

$z = 1.1508$ . The sub-DLA at  $z = 1.1508$  is a very complex system, spanning  $800 \text{ km s}^{-1}$  for absorption in many low-ionization transitions. It has many molecular hydrogen lines detected. Our identifications for the molecules follow exactly those of Reimers et al. (2003). The saturated region of the sub-DLA profile spans  $\sim 1100 \text{ km s}^{-1}$ . A separate component at  $\sim -900 \text{ km s}^{-1}$  is likely also to be Ly $\alpha$ , but with no associated metals in the *HST*/*STIS* spectrum. Many neutral species of C I and N I are detected in a single, narrow component at  $\sim 0 \text{ km s}^{-1}$ , presumably associated with the bulk of the H I. Features

at other velocities seen in the neutral transition panels in Fig. 20 are not related to this system (see line identifications in Table 3). O I 1302 is blended with Ly $\alpha$  at  $z = 1.3039$ , and cannot be measured, and no other strong O I transitions are covered. Many singly ionized transitions are detected for the system, both in the  $0 \text{ km s}^{-1}$  component and at many other velocities to the blue. These match the Mg II and Fe II from the VLT/*UVES* spectrum (Levshakov et al. 2003). Strong Si III absorption is detected in many components, spanning the full velocity range. Si IV  $\lambda\lambda 1394, 1403$  is detected as well, but there appears to be significant blending with Si IV  $\lambda 1394$ , because Si IV  $\lambda 1403$  is much weaker at some velocities. C IV  $\lambda\lambda 1548, 1551$  is also detected in the VLT/*UVES* spectrum. N V  $\lambda\lambda 1239, 1243$  is covered, but not detected, and O VI  $\lambda\lambda 1032, 1038$  is not covered.

$z = 1.3849$ . An O VI doublet detected in the *HST*/*STIS* spectrum at  $z = 1.3849$  has its  $\lambda 1038$  member blended to the blue with Ly $\beta$  at 1.4124. C IV  $\lambda\lambda 1548, 1551$  is detected at the same redshift in the VLT/*UVES* spectrum (Levshakov et al. 2003). The corresponding, relatively weak (unsaturated) Ly $\alpha$  line lies blueward of a larger saturated Ly $\alpha$  feature. C III may also be detected.

$z = 1.4163$ . There is a possible O VI system at  $z = 1.4163$ , as reported by Levshakov et al. (2003), however neither member of the O VI doublet aligns with the Ly $\alpha$  and Ly $\beta$ , which are also detected in the *STIS* spectrum. There could be C III associated with this system, but it is badly blended with a probable Ly $\alpha$  line, thus its alignment cannot be verified. Therefore, there is not convincing evidence for detected metals in this system.

$z = 1.6020$ . The O VI system at  $z = 1.6020$  is well aligned and is detected in Ly $\beta$  and Ly $\gamma$  in the *HST*/*STIS* spectrum. Ly $\alpha$ , and possibly C IV, is detected in the VLT/*UVES* spectrum (Levshakov et al. 2003).

$z = 1.6668$ . There is a possible O VI system at  $z = 1.6668$ , though its identity is somewhat uncertain. O VI  $\lambda 1038$  is blended with a possible Ly $\alpha$  line, such that the profiles of the doublet members cannot be compared. Ly $\beta$  is not detected at the position, however Ly $\alpha$  is detected, with about the same profile shape and equivalent width as the O VI. Thus, this could be a fairly typical associated O VI absorber.

$z = 1.6736$ . There is an O VI system at  $z = 1.6736$  detected in the *HST*/*STIS* spectrum. O VI  $\lambda 1038$  is blended to the red with a possible Ly $\alpha$  line. Ly $\beta$  is detected, as are higher order Lyman series lines, but the latter are blended with other transitions (see Table 3). C IV  $\lambda\lambda 1548, 1551$  and Ly $\alpha$  are detected in the VLT/*UVES* spectrum (Levshakov et al. 2003).

$z = 1.6971$ . The associated O VI absorber at  $z = 1.6971$  also has C III  $\lambda 977$  and probably S VI  $\lambda 933$  detected. Levshakov et al. (2003) also detected Ly $\alpha$ , Si IV  $\lambda\lambda 1394, 1403$ , C IV  $\lambda\lambda 1548, 1551$  and N V  $\lambda\lambda 1239, 1243$  in their VLT/*UVES* spectrum. The Ly $\alpha$  profile is not black, again a signature of associated O VI absorbers.

$z = 1.7358$ . A possible O VI system at  $z = 1.7358$  cannot be confirmed by other features in the *HST*/*STIS* spectrum. Although Ly $\beta$  is covered, it is blended with Galactic Mg II  $\lambda 2803$ . If real, this system would be significantly redshifted relative to the emission redshift of the quasar.

### 3.3 PG 1206+459 ( $z_{\text{em}} = 1.16254$ )

This quasar was observed by *HST*/*FOS* as part of the Quasar Absorption Line Key Project, but they had difficulty in identifying many of the lines due to uncertain continuum fitting (Jannuzi et al. 1998). They found evidence for an extensive metal-line system separated into subsystems at  $z = 0.9254, 0.9277$  and  $0.9342$ , even at low resolution. Churchill et al. (1999) modelled this system based on

the *HST*/FOS data, along with Keck/HIRES data (Churchill & Vogt 2001). Ding et al. (2003) refined these models once the *HST*/STIS spectra were available.

Churchill et al. (1999) observed this quasar with *HST*/STIS to facilitate a detailed study of the systems at  $z \sim 0.927$ . The *HST*/STIS spectrum covers the Ly $\alpha$  forest blueward of 2628 Å, but does not cover any higher order Lyman series lines. There are only three metal-line systems found in the *HST*/STIS spectrum: the extensive metal-line system at  $z \sim 0.927$  mentioned above, a C IV system, and an associated N V system. Figs 28–32 presents system plots for these metal-line systems, detected towards PG 1206+459.

$z = 0.7338$ . There is a weak C IV doublet at  $z = 0.7338$ . The C IV  $\lambda 1548$  is blended with Si IV  $\lambda 1394$  from the subsystem at  $z = 0.9254$ , and also to the red with an unknown blend, probably Ly $\alpha$ . The large feature blueward of the C IV  $\lambda 1551$  transition is Si IV  $\lambda 1394$  at  $z = 0.9276$ . Mg II is not detected in the Keck/HIRES spectrum, nor any other low-ionization transitions in the *HST*/STIS spectrum. However, the system is confirmed by Ly $\alpha$  in the *HST*/FOS spectrum.

$z = 0.9254$ . The complex metal-line system at  $z = 0.9277$  is spread over more than 1000 km s<sup>-1</sup>. Ding et al. (2003) separated it into three systems at  $z = 0.9254$  (System A),  $z = 0.9277$  (System B) and  $z = 0.9342$  (System C). They suggest that these systems are produced by three different galaxies in a group. System A, at  $z = 0.9254$ , has detected C II, Si III, Si IV  $\lambda\lambda 1394, 1403$ , C IV  $\lambda\lambda 1548, 1551$  and N V  $\lambda\lambda 1239, 1243$  in the *HST*/STIS spectrum. Many other transitions, including O VI  $\lambda\lambda 1032, 1038$  and Lyman series lines, were detected in the *HST*/FOS spectrum. Si IV  $\lambda 1394$  is blended with C IV  $\lambda 1548$  from the  $z = 0.7338$  C IV system. Ly $\alpha$  is saturated and covers the entire velocity range between this system and System B.

$z = 0.9276$ . System B, at  $z = 0.9276$ , produces a partial Lyman limit break in the *HST*/FOS spectrum. It is detected in several transitions of Si II, C II, Si III, Si IV  $\lambda\lambda 1394, 1403$ , C IV  $\lambda\lambda 1548, 1551$  and N V  $\lambda\lambda 1239, 1243$ . Galactic Fe II  $\lambda 2344$  is blended with the red wing of the Ly $\alpha$  profile. C II  $\lambda 1335$  is blended to the red with an unidentified line, probably Ly $\alpha$ . The feature redward of Si IV  $\lambda 1394$  is C IV  $\lambda 1551$  from the  $z = 0.7338$  system. C IV is self-blended, with the C IV  $\lambda 1551$  from System A superimposed on the C IV  $\lambda 1548$  from System B.

$z = 0.9343$ . System C, at  $z = 0.9343$  is unusual in its high velocity relative to the main system, System B. For this system, which would be considered a single-cloud, weak Mg II absorber if isolated from the other systems, is detected in Ly $\alpha$ , Si II, C II, Si III, Si IV  $\lambda\lambda 1394, 1403$  and C IV  $\lambda\lambda 1548, 1551$ . N V  $\lambda 1239$  is blended with N V  $\lambda 1243$  from System B, but N V  $\lambda 1243$  is not detected in a clean part of the spectrum. Again, O VI and various other transitions are detected in the *HST*/FOS spectrum.

$z = 1.0281$ . The N V system at  $z = 1.0281$  is almost certainly intrinsic judging by its broad profile and the ‘non-black’ Ly $\alpha$  line, evidence for partial covering. No other metals are detected besides the N V.

### 3.4 PG 1241+176 ( $z_{\text{em}} = 1.273$ )

This was also a quasar studied for the Quasar Absorption Line Key Project (Jannuzi et al. 1998), and a Keck/HIRES spectrum was obtained by Churchill & Vogt (2001). Particular Mg II systems, with optical and UV coverage, were studied in Churchill et al. (2000). The  $z = 0.5505, 0.5584$  and  $0.8954$  systems were modelled in detail by Ding, Charlton & Churchill (2005).

This quasar was observed with *HST*/STIS by Churchill et al. in order to provide constraints on the physical conditions in Mg II ab-

sorbers. Ly $\alpha$  forest lines appear in *HST*/STIS spectrum quasar spectrum blueward of 2763 Å, and the Ly $\beta$  forest is covered blueward of 2332 Å. We find evidence for six metal-line systems: one strong Mg II absorber, two weak Mg II absorbers, one weak C IV and two associated O VI absorbers. The system plots for these metal-line systems are shown in Figs 33–38.

$z = 0.5507$ . Jannuzi et al. (1998) found a metal-line system at  $z = 0.5507$  with strong C IV detected. This system corresponds to a strong Mg II absorber detected in a Keck/HIRES spectrum (Churchill & Vogt 2001), which also has detected Ca II, Fe II and Mg I. In the *HST*/STIS spectrum, we also find Fe II  $\lambda 1608$ , Al II  $\lambda 1671$  and C IV  $\lambda\lambda 1548, 1551$ . There is a  $3\sigma$  detection of Al II  $\lambda 1671$  at  $v \sim 150$  km s<sup>-1</sup>, which coincides with a satellite component of Mg II  $\lambda\lambda 2796, 2803$  in the Keck/HIRES spectrum (Ding et al. 2005).

$z = 0.5584$ . For the multiple-cloud, weak Mg II absorber at  $z = 0.5584$ , C IV  $\lambda\lambda 1548, 1551$  was detected in the *HST*/STIS spectrum, but no low-ionization transitions were detected, though Al II  $\lambda 1671$ , Al III  $\lambda\lambda 1855, 1863$  and Si II  $\lambda 1527$  were covered.

$z = 0.7577$ . A possible weak C IV doublet at  $z = 0.7577$  cannot be confirmed, since Ly $\alpha$  is not covered in the *HST*/STIS or in the previous *HST*/FOS spectrum.

$z = 0.8954$ . The single-cloud, weak Mg II absorber at  $z = 0.8954$  has detected Ly $\alpha$ , Si III  $\lambda 1207$ , Si IV  $\lambda 1394$  and C IV  $\lambda\lambda 1548, 1551$ . The Si IV  $\lambda 1403$  is affected by a blend. Although there is a detection at the position of Si II  $\lambda 1260$ , Ding et al. (2005) note that this may be a blend, since it is difficult to explain the strength of this feature in comparison to the weaker Mg II  $\lambda\lambda 2796, 2803$  lines.

$z = 1.2152$ . The O VI system, at  $z = 1.2152$ , found by Jannuzi et al. (1998) is confirmed here, showing O VI  $\lambda\lambda 1032, 1038$  and Ly $\alpha$  in the *HST*/STIS spectrum. Although a feature is detected at the position of N V  $\lambda 1239$ , also noted by Jannuzi et al. (1998), this is inconsistent with the lack of detection of N V  $\lambda 1243$ , and so cannot be confirmed.

$z = 1.2717$ . Jannuzi et al. (1998) found a strong associated O VI absorber at  $z = 1.2717$  in their *HST*/FOS spectrum, for which Ly $\alpha$  and Ly $\beta$  were also detected. In the higher resolution *HST*/STIS spectrum, we confirm these detections, but do not find any other associated absorption. The relatively weak Ly $\alpha$ , as compared to O VI  $\lambda\lambda 1032, 1038$  is characteristic of a class of associated O VI absorbers (Ganguly et al., in preparation).

### 3.5 PG 1248+401 ( $z_{\text{em}} = 1.030$ )

This quasar was studied by the *HST* Quasar Absorption Line Key Project using G190H and G270H spectra obtained with FOS (Jannuzi et al. 1998), who found metal-line systems at  $z = 0.3946, 0.7660, 0.7732$  and  $0.8553$ . The latter two systems correspond to strong Mg II absorbers, modelled by Ding et al. (2005) based on Keck/HIRES data (Churchill & Vogt 2001) and the *HST*/STIS spectrum presented here. Another system, at  $z = 0.7011$ , with only C IV  $\lambda\lambda 1548, 1551$  and Ly $\alpha$  detected, was discussed in Milutinović et al. (2006).

Churchill et al. (1999) obtained a spectrum of this quasar with *HST*/STIS in order to provide constraints on the physical conditions in the two strong Mg II absorbers along the line of sight. In the *HST*/STIS spectrum, the Ly $\alpha$  forest is only covered up to a wavelength of 2468 Å, and higher order Lyman series lines are not covered. We find evidence for two strong Mg II and two weak C IV systems in the *HST*/STIS spectra. These systems are shown in Figs 39–45.

$z = 0.3946$ . Al II  $\lambda 1671$  and Al III  $\lambda 1855$  are the only prominent transitions from the possible  $z = 0.3946$  system that are covered in the *HST/STIS* spectrum. Although there is a detection at the position of Al II  $\lambda 1671$ , the lack of detected Al III  $\lambda \lambda 1855, 1863$  and the lack of detection of C IV  $\lambda \lambda 1548, 1551$  in the FOS spectrum leads us to question the reality of this system. Thus we prefer an identification of the feature at  $2330.09 \text{ \AA}$  as Ly $\alpha$ .

$z = 0.5648$ . A C IV doublet is found at  $z = 0.5648$  in the *HST/STIS* spectrum. It is confirmed by a Ly $\alpha$  detection in the G190H *HST/FOS* spectrum (Jannuzi et al. 1998). The weak feature at the expected position of Si II  $\lambda 1527$  is unlikely to be Si II because of the absence of the stronger Si II  $\lambda 1260$  transition in the FOS spectrum.

$z = 0.6174$ . There is a very weak possible C IV doublet at  $z = 0.6174$  in the *HST/STIS* spectrum, however the alignment is not perfect. Also, there is no Ly $\alpha$  detected in the FOS spectrum to a rest-frame equivalent width limit of  $0.11 \text{ \AA}$ .

$z = 0.7011$ . The C IV absorption system at  $z = 0.7011$  is confirmed by a Ly $\alpha$  detection in the FOS spectrum, but there are no additional detections in the *HST/STIS* spectrum.

$z = 0.7728$ . The strong Mg II system at  $z = 0.7728$  has detected Al II  $\lambda 1671$ , Si II  $\lambda 1304$  and Si II  $\lambda 1527$ , C II  $\lambda 1335$ , Si IV  $\lambda \lambda 1394, 1403$  and C IV  $\lambda \lambda 1548, 1551$  in the STIS E230M spectrum. O I  $\lambda 1302$  may be detected in the strongest low-ionization component, but the spectrum is very noisy in that region.

$z = 0.7760$ . We cannot confirm a system at  $z = 0.7760$ , which was suggested by Jannuzi et al. (1998), however we note that we also do not detect C IV  $\lambda \lambda 1548, 1551$  to a  $3\sigma$  rest-frame equivalent width limit of  $0.02 \text{ \AA}$ . It is still possible that this system exists, but is collisionally ionized, as proposed by Jannuzi et al. (1998).

$z = 0.8545$ . The strong Mg II system at  $z = 0.8545$  has detected Si II  $\lambda 1260$ , C II  $\lambda 1335$ , Si IV  $\lambda \lambda 1394, 1403$ , C IV  $\lambda \lambda 1548, 1551$  and N V  $\lambda \lambda 1239, 1243$ . Kinematically, this system is interesting, with satellite components in low-ionization gas (offset  $\sim 300 \text{ km s}^{-1}$  from the main absorption) having corresponding, broader C IV absorption.

### 3.6 CSO 873 ( $z_{\text{em}} = 1.022$ )

This quasar was previously studied through G190H and G270H *HST/FOS* spectra (Bahcall et al. 1996), but only three metal-line systems were indicated, at  $z = 0.2891, 0.6606$  and  $1.0022$ . The  $z = 0.6606$  coincides with a strong Mg II absorber (Churchill & Vogt 2001), and it was modelled by Ding et al. (2005).

The *HST/STIS* spectrum was obtained in a programme (PI Churchill) to facilitate a study of the  $z = 0.6606$  Mg II absorber. This spectrum covers the Ly $\alpha$  forest up to a wavelength of  $2458 \text{ \AA}$ , and does not cover any Ly $\beta$  lines.

$z = 0.6611$ . Besides Galactic absorption, in the *HST/STIS* E230M spectrum, we detect metal-line absorption from only the system at  $z = 0.6611$ , which corresponds to a full Lyman limit break seen in a *HST/FOS* G160L spectrum (Bahcall et al. 1993, 1996). A system plot is shown in Fig. 46. From this system we find Al II  $\lambda 1671$ , Si II  $\lambda 1527$  and C IV  $\lambda \lambda 1548, 1551$ . Si IV is not detected. In fact, the C IV absorption at the velocity of the low-ionization absorption is relatively weak, and this system classifies as ‘C IV-deficient’ (Ding et al. 2005). The strongest C IV absorption is  $\sim 200 \text{ km s}^{-1}$  redward of the strongest low-ionization component. Jannuzi et al. (1998) note a complex of Ly $\alpha$  lines ranging from  $z = 0.6692$  to  $0.6771$ . They found no metals associated with this complex in the low-resolution *HST/FOS* spectrum. We note that with the STIS data, it is possible to set a stronger limit, with a rest-frame  $3\sigma$  equivalent width limit  $W_r(1548) < 0.02\text{ \AA}$ .

### 3.7 PG 1634+706 ( $z_{\text{em}} = 1.334$ )

This was one of the *HST* QSO Absorption Line Key Project quasars, and its *HST/FOS* G270M spectrum was presented in Bahcall et al. (1996). In that spectrum, three extensive metal-line systems are present at  $z = 0.9060, 0.9908$  and  $1.0417$ . Also, there are possible C IV doublets at  $z = 0.5582, 0.6540, 0.6790$  and  $0.7796$ , and a possible O VI doublet at  $z = 1.3413$ . In a Keck/HIRES optical spectrum, strong Mg II absorption is detected from the  $z = 0.9908$  system, and weak Mg II absorption from the  $z = 0.6540, 0.9060$  and  $1.0417$  systems (Churchill et al. 1999; Churchill & Vogt 2001; Charlton et al. 2003). Weak Mg II is also detected at  $z = 0.8181$  in the optical spectrum (Churchill et al. 1999). The three single-cloud, weak Mg II absorbers at  $z = 0.8181, 0.9056$  and  $0.6534$  were modelled by Charlton et al. (2003), the multiple-cloud, weak Mg II absorber at  $z = 1.0414$  by Zonak et al. (2004), and the strong Mg II absorber at  $z = 0.9902$  by Ding et al. (2003).

Two programmes contribute different wavelength coverage of this quasar with *HST/STIS*. Burles (1997a) observed the quasar in order to measure the primordial deuterium-to-hydrogen ratio (D/H). Jannuzi et al. (1998) provided redward coverage in order to conduct a detailed study of the Ly $\alpha$  forest. In the *HST/STIS* spectra, Ly $\alpha$  is covered up to  $2837 \text{ \AA}$ , Ly $\beta$  up to  $2395 \text{ \AA}$  and Ly $\gamma$  in the small region up to  $2268 \text{ \AA}$ . There is detected absorption from the strong Mg II absorber, and from the four weak Mg II absorbers mentioned above. There are also several possible C IV systems and a possible O VI system, as well as an interesting ‘C III/Si III-only’ system. There is a possible intrinsic N V system and an associated O VI system observed towards this quasar as well. We report on these systems here, and shown system plots in Figs 47–56.

$z = 0.2854$ . We can only tentatively claim a C IV doublet at  $z = 0.2854$ . The C IV  $\lambda 1548$  and C IV  $\lambda 1551$  profiles match reasonably well, but C IV  $\lambda 1551$  may be a bit too strong at some velocities, and there is no coverage of transitions that could confirm this identification. This could relate to a blend with the C III  $\lambda 977$  from the  $z = 1.0415$  system (see below).

$z = 0.6513$ . There is also a probable, narrow C IV doublet at  $z = 0.6513$ . The C IV  $\lambda 1550$  transition is blended with C IV  $\lambda 1548$  from the  $z = 0.6535$  system. If this is real, it is unusual in the weakness of Ly $\alpha$  relative to C IV. A weak, narrow N V doublet may also be detected.

$z = 0.6535$ . The *HST/STIS* spectrum shows weak absorption in several low and intermediate transitions related to the  $z = 0.6535$  single-cloud, weak Mg II absorber. The C IV has two components redward of the dominant low-ionization absorption, and Si IV is weaker but has similar kinematics.

$z = 0.8182$ . The single-cloud, weak Mg II absorber at  $z = 0.8182$  has detected Si II, C II, Si IV and C IV absorption, all centred at the same velocity as the Mg II. Si III  $\lambda 1206$  is blended with Ly $\beta$  from a system at  $z = 1.1382$ , and is apparent as a small depression in the red wing of that feature.

$z = 0.9056$ . For another single-cloud, weak Mg II absorber at  $z = 0.9056$ , Ly $\alpha$ , Ly $\beta$ , C II, Si II, Si IV, C IV, N V and O VI are detected in the *HST/STIS* spectrum. The coverage of N V and O VI is unusual for single-cloud, weak Mg II absorbers and is important for considerations of the phase structure of these objects.

$z = 0.9645$ . There is an interesting system detected in the *HST/STIS* spectrum at  $z = 0.9645$ . Most of the common metal transitions have good coverage, but only C III and Si III are detected. Ly $\alpha$  and Ly $\beta$  confirm the reality of this system.

$z = 0.9904$ . The C IV-deficient, strong Mg II absorber at  $z = 0.9904$  has detections in the *HST/STIS* spectrum of the first four

Lyman series lines, O I, and a variety of singly to triply ionized transitions, including relatively weak C IV absorption. N V and O VI are covered, but not detected. The Ly $\delta$  line is detected, but suffers from a blend to the blue with H I  $\lambda$ 926 from the system at  $z = 1.0415$ . This system is of interest because the higher ionization transitions appear redward of the lower ionization transitions, indicating a density gradient across the system (Ding et al. 2005).

$z = 1.0415$ . The  $z = 1.0415$  multiple-cloud, weak Mg II system has a partial Lyman limit break detected in a *HST/STIS* G230M spectrum. The higher order Lyman series lines are detected down to the break in the *HST/STIS* E230M spectrum, though past H I  $\lambda$ 919 they suffer badly from blending with the Lyman series lines from the  $z = 0.9904$  system. Metal lines are detected in Si II, C II, Si III, Si IV and O VI from each of two subsystems. The low-ionization transitions are centred at different velocities than the high-ionization transitions. C III  $\lambda$ 977 is also detected, but may be blended with the possible C IV doublet at  $z = 0.2854$ . C IV is detected in a low-resolution *HST/FOS* spectrum, but is redward of the *HST/STIS* coverage.

$z = 1.1408$ . There is a possible O VI absorber at  $z = 1.1408$ , however its O VI  $\lambda$ 1032 transition is too strong relative to the O VI  $\lambda$ 1038 transition. Although Ly $\alpha$ , Ly $\beta$  and Ly $\gamma$  are detected at this velocity, their relative strengths are also inconsistent, perhaps due to unknown blends.

$z = 1.3413$ . An O VI doublet is detected from a system at  $z = 1.3413$ , which is slightly redward of  $z_{\text{em}}$ . It is confirmed by a very weak Ly $\alpha$  detection, but Ly $\beta$  is badly blended and provides no additional constraint. This is another example of an associated O VI system (e.g. Ganguly et al., in preparation).

### 3.8 PG 1718+481 ( $z_{\text{em}} = 1.084$ )

The E230M observation of this quasar with *HST/STIS* was proposed by Bures (1997b) to facilitate a study of the D/H in a system at  $z = 0.701$  (Kirkman et al. 2001). An *HST/STIS* G230M spectrum was also obtained, covering the Lyman series for this system (Kirkman et al. 2001). Earlier, this quasar was observed as part of the *HST* Quasar Absorption Line Key Project. Jannuzi et al. (1998) found metal-line systems at  $z = 0.8929$ , 1.0323 and 1.0872.

In the *HST/STIS* spectrum, Ly $\alpha$  is covered up to 2535 Å, Ly $\beta$  up to 2138 Å and Ly $\gamma$  up to 2036 Å. All Lyman series lines are covered below 1902 Å. In addition to the  $z = 0.701$  system, for which this observation was obtained, we find evidence for four definite and two possible O VI absorbers. These systems are all shown in Figs 57–64.

$z = 0.7011$ . The  $z = 0.7011$  Lyman limit system has Ly $\alpha$  and Si III detected in the *HST/STIS* spectrum. Weak C II  $\lambda$ 1335 also appear to be detected, consistent with the weak Mg II absorption that Kirkman et al. (2001) found in a HIRES/Keck spectrum. C IV  $\lambda\lambda$ 1548, 1551 and Si IV  $\lambda\lambda$ 1394, 1403 are covered, but not detected.

$z = 0.8928$ . An O VI absorber is found at  $z = 0.8928$  in the STIS spectrum, accompanied by detections of Si III, Ly $\alpha$  and Ly $\beta$ . Jannuzi et al. (1998) also found C III in a low-resolution *HST/FOS* spectrum.

$z = 1.0065$ . Another O VI system is detected at  $z = 1.0065$  in the *HST/STIS* spectrum. Ly $\alpha$  and Ly $\beta$  are also detected, confirming this O VI doublet.

$z = 1.0318$ . A stronger O VI absorber is detected at  $z = 1.0318$ , corresponding to the system found by Jannuzi et al. (1998). In the *HST/STIS* spectrum the first five Lyman series lines are detected, along with C III, N V  $\lambda\lambda$ 1239, 1243 and O VI  $\lambda\lambda$ 1032, 1038.

$z = 1.0507$ . There is a feature detected (just above  $5\sigma$ ) at the position of O VI  $\lambda$ 1032 for a system at  $z = 1.0507$  with detected Ly $\alpha$  and Ly $\beta$  absorption. The O VI  $\lambda$ 1038 is not detected, even at

$2\sigma$ , so it is uncertain whether there are detected metals for this system.

$z = 1.0548$ . The  $z = 1.0548$  system, with Ly $\alpha$ , Ly $\beta$ , Ly $\gamma$  and Ly $\delta$  detected in the *HST/STIS* spectrum, appears to be an O VI absorber, with weak C III absorption. The O VI doublet cannot be confirmed because the O VI  $\lambda$ 1032 member is blended with Ly $\beta$  at  $z = 1.0674$ .

$z = 1.0867$ . There is an associated system with  $z = 1.0867$ , detected in Ly $\alpha$ , Ly $\beta$  and Ly $\gamma$ . The Ly $\alpha$  profile has a black, saturated region at this redshift. The  $z = 1.0867$  component has detections in C III and Si III.

$z = 1.0874$ . There is also a non-black component at  $z = 1.0874$ . This system detected O VI  $\lambda\lambda$  1032, 1038, and resembles many other associated O VI systems.

## 4 SUMMARY OF SYSTEMS

This paper presents a catalogue that is useful for investigations of metal-line systems and the Ly $\alpha$  forest in eight of the highest S/N E230M spectra from the *HST/STIS* archive. ASCII files listing the full spectra of the eight quasars are available in the electronic version (sample is presented in Table 4). We have identified a total of 56 metal-line systems (with at least one metal line detected) towards the eight quasars listed in Table 1, as presented in Figs 9–64. For key transitions, Table 5 tabulates in how many of the 56 systems a given transition was covered and in how many it was detected. We must caution that clearly these numbers apply only to this particular data set and are highly dependent on the detection limits of the spectra, to the exact wavelength coverage, and to biases towards certain kinds of quasars for the sample. In this sample of eight quasars, there may be a preference towards strong low-ionization absorbers, since many of them were chosen for a programme to study the C IV associated with Mg II absorption (see Table 1).

None the less, it is useful to note from Table 5 that for about half of the 56 systems we have coverage of the C IV and O VI doublets, and that in those cases these high-ionization transitions were detected  $\sim 90$  per cent of the time. Intermediate ionization transitions such as C III  $\lambda$ 977 and Si III  $\lambda$ 1207 were also covered about half the time, and were detected in 50/58 per cent of the sightlines, respectively. C II  $\lambda$ 1335 is also covered for about half of the systems, and was detected 56 per cent of the time, while Si II  $\lambda$ 1260 was only detected in 36 per cent of the sightlines for which it was covered. We conclude that almost all  $1 < z < 1.7$  metal-line systems have high-ionization absorption detected, but that only half have detected low-ionization absorption. These numbers are consistent with the findings of Milutinović et al. (2006) that half of all C IV absorbers

**Table 4.** Sample – ASCII data of eight quasars.<sup>a</sup>

$\lambda_{\text{obs}}$	Flux PG 0117 + 213	$\sigma(\text{flux})$
2278.709 96	0.149 91	0.185 15
2278.747 56	0.031 87	0.188 36
2278.784 91	0.384 73	0.192 94
2278.822 51	−0.246 22	0.184 88
2278.860 11	0.839 85	0.184 44
2278.897 46	0.270 36	0.185 83
2278.934 81	0.541 64	0.184 63
2278.972 41	0.597 44	0.190 27
2279.010 01	0.773 54	0.190 77
2279.047 36	0.982 99	0.196 21

<sup>a</sup>Full spectra of the eight quasars are available in the electronic version (see the Supplementary Material section).

**Table 5.** Detection rate of important transitions.

Transition	# <sub>cov</sub> <sup>a</sup>	# <sub>det</sub> <sup>b</sup>	Detection rate <sup>c</sup> (per cent)
C II $\lambda$ 1335	27	15	56
C III $\lambda$ 977	26	13	50
C IV $\lambda$ 1548	26	23	88
N II $\lambda$ 1084	31	1	3
N V $\lambda$ 1239	37	9	24
O VI $\lambda$ 1032	30	27	90
Al II $\lambda$ 1671	18	7	39
Al III $\lambda$ 1855	10	2	20
Si II $\lambda$ 1260	36	13	36
Si III $\lambda$ 1207	36	21	58
Si IV $\lambda$ 1394	26	13	50
Fe II $\lambda$ 1608	22	2	9

<sup>a</sup>Number of systems in which transition is covered; <sup>b</sup>number of systems in which transition is detected; <sup>c</sup>probability that transition is detected at  $>5\sigma$  for system in which it is covered.

at low redshift have detected low-ionization absorption (sometimes weak), and that the other half do not. This is not surprising since the samples used for these studies have considerable overlap. However, these detection rates are redshift dependent, and could be different at higher redshift.

Studies of the statistics of the Ly $\alpha$  forest can be significantly affected by metal lines in the forest. With our catalogue we are able to give an indication of the level of contamination by metal lines in the  $1.0 < z < 1.7$  forest. Specifically, we scanned the wavelength regions of our catalogue that are in the Ly $\alpha$  forest of the quasar, but are redward of the Ly $\beta$  forest. Table 1 lists how many Ly $\alpha$  lines and how many metal lines were detected in this region for each quasar. It also shows that 9–10 of the features detected in the E230M quasar spectra are actually Galactic absorption. We conclude that of the  $1.0 < z < 1.7$  Ly $\alpha$  forest lines detected towards each of the quasars (redward of the Ly $\beta$  forest), 20–33 per cent of the lines in the Ly $\alpha$  forest are actually metal lines. This ‘contamination’ is significant enough that it is important to remove it before computing the statistics of the Ly $\alpha$  lines, and is clearly itself a complicated function of redshift.

## ACKNOWLEDGMENTS

We acknowledge support from NASA under grant NAG5-6399 NNG04GE73G and by the National Science Foundation under grant AST 04-07138. JRM and RSL were partially funded by the NSF Research Experience for Undergraduates (REU) programme. DT and DK were supported in part by STScI grants HST-AR-10688 and HST-AR-10288. SB was supported by the NSF/REU programme in the summer of 2005. We also thank the anonymous referee for useful comments and suggestions.

## REFERENCES

- Bahcall J. N. et al., 1993, *ApJS*, 87, 1  
 Bahcall J. N. et al., 1996, *ApJ*, 457, 19  
 Brown T. et al., 2002, in Mobasher B., ed., *HST STIS Data Handbook*, version 4.0. Space Telescope Science Institute, Baltimore  
 Burles S., 1997a, *HST*, Proposal, 3635  
 Burles S., 1997b, *HST*, Proposal, 7292  
 Charlton J. C., Ding J., Zonak S. G., Churchill C. W., Bond N. A., Rigby J. R., 2003, *ApJ*, 589, 311  
 Churchill C. W., Vogt S. S., 2001, *AJ*, 122, 679

- Churchill C. W., Rigby J. R., Charlton J. C., Vogt S. S., 1999, *ApJS*, 120, 51  
 Churchill C. W., Mellon R. R., Charlton J. C., Jannuzi B. T., Kirhakos S., Steidel C. C., Schneider D. P., 2000, *ApJS*, 130, 91  
 Ding J., Charlton J. C., Churchill C. W., Palma C., 2003a, *ApJ*, 590, 746  
 Ding J., Charlton J. C., Bond N. A., Zonak S. G., Churchill C. W., 2003b, *ApJ*, 587, 551  
 Ding J., Charlton J. C., Churchill C. W., 2005, *ApJ*, 621, 615  
 Jannuzi B. T. et al., 1998, *ApJS*, 118, 1  
 Kirkman D. et al., 2001, *ApJ*, 559, 23  
 Kirkman D., Tytler D., Lubin D., Charlton J., 2007, *MNRAS*, 376, 1227  
 Koratkar A., Antonucci R., Goodrich R., Storrs A., 1998, *ApJ*, 503, 599  
 Levshakov S. A., Agafonova I. I., Reimers D., Baade R., 2003, *A&A*, 404, 449  
 Masiero J. R., Charlton J. C., Ding J., Churchill C. W., 2005, *ApJ*, 623, 57  
 Milutinović N., Rigby J. R., Masiero J. R., Lynch R. S., Palma C., Charlton J. C., 2006, *ApJ*, 641, 190  
 Narayanan A., Charlton J. C., Masiero J. R., Lynch R., 2005, *ApJ*, 632, 92  
 Rao S. M., Turnshek D. A., 2000, *ApJS*, 130, 1  
 Reimers D., Baade R., Quast R., Levshakov S. A., 2003, *A&A*, 410, 785  
 Savage B. D., Sembach K. R., Tripp T. M., Richter P., 2002, *ApJ*, 564, 631  
 Schneider D. P. et al., 1993, *ApJS*, 87, 45  
 Tripp T. M., Savage B. D., Jenkins E. B., 2000, *ApJ*, 534, L1  
 Verner D. A., Verner E. M., Ferland G. J., 1996, *At. Data Nucl. Data Tables*, 64, 1  
 Zonak S. G., Charlton J. C., Ding J., Churchill C. W., 2004, *ApJ*, 606, 196

## SUPPLEMENTARY MATERIAL

The following supplementary material is available for this article.

**Table 3.** Features with  $5\sigma$  identified in the *HST/STIS* E230M spectra of eight quasars.

**Table 4.** ASCII files of eight quasars.

**Figure 1.** Normalized flux versus wavelength for a portion of the *HST/E230M* spectrum of quasar PG 0117+213, as in Fig. 1.

**Figure 2.** Normalized flux versus wavelength for a portion of the *HST/E230M* spectrum of quasar HE 0515–4414, as in Fig. 1.

**Figure 3.** Normalized flux versus wavelength for a portion of the *HST/E230M* spectrum of quasar PG 1206+459, as in Fig. 1.

**Figure 4.** Normalized flux versus wavelength for a portion of the *HST/E230M* spectrum of quasar PG 1241+176, as in Fig. 1.

**Figure 5.** Normalized flux versus wavelength for a portion of the *HST/E230M* spectrum of quasar PG 1248+401, as in Fig. 1.

**Figure 6.** Normalized flux versus wavelength for a portion of the *HST/E230M* spectrum of quasar CSO 873, as in Fig. 1.

**Figure 7.** Normalized flux versus wavelength for a portion of the *HST/E230M* spectrum of quasar PG 1634+706, as in Fig. 1.

**Figure 8.** Normalized flux versus wavelength for a portion of the *HST/E230M* spectrum of quasar PG 1718+481, as in Fig. 1.

**Figure 9.** System plot for the  $z = 0.5764$  system towards PG 0117+213. Important transitions are plotted, unless they are so badly compromised by a blend that no useful constraints can be gathered. The transitions are aligned in velocity space, with  $0 \text{ km s}^{-1}$  corresponding to  $z = 0.5764$ . The error spectrum is plotted beneath the data, and a dashed line shown at zero flux.

**Figure 10.** System plot for the  $z = 0.7290$  system towards PG 0117+213, as described in Fig. 9.

**Figure 11.** System plot for the  $z = 1.0480$  system towards PG 0117+213, as described in Fig. 9.

**Figure 12.** System plot for the  $z = 1.3250$  system towards PG 0117+213, as described in Fig. 9.

**Figure 13.** System plot for the  $z = 1.3390$  system towards PG 0117+213, as described in Fig. 9.

**Figure 14.** System plot for the  $z = 1.3430$  system towards PG 0117+213, as described in Fig. 9.

**Figure 15.** System plot for the  $z = 1.4242$  system towards PG 0117+213, as described in Fig. 9.

**Figure 16.** System plot for the  $z = 1.4463$  system towards PG 0117+213, as described in Fig. 9.

**Figure 17.** System plot for the  $z = 1.4478$  system towards PG 0117+213, as described in Fig. 9.

**Figure 18.** System plot for the  $z = 1.5088$  system towards PG 0117+213, as described in Fig. 9.

**Figure 19.** System plot for the  $z = 0.9406$  system towards HE 0515–4411, as described in Fig. 9.

**Figure 20.** System plot for the  $z = 1.1508$  system towards HE 0515–4411, as described in Fig. 9.

**Figure 21.** System plot for the  $z = 1.3849$  system towards HE 0515–4411, as described in Fig. 9.

**Figure 22.** System plot for the  $z = 1.4163$  system towards HE 0515–4411, as described in Fig. 9.

**Figure 23.** System plot for the  $z = 1.6020$  system towards HE 0515–4411, as described in Fig. 9.

**Figure 24.** System plot for the  $z = 1.6668$  system towards HE 0515–4411, as described in Fig. 9.

**Figure 25.** System plot for the  $z = 1.6736$  system towards HE 0515–4411, as described in Fig. 9.

**Figure 26.** System plot for the  $z = 1.6971$  system towards HE 0515–4411, as described in Fig. 9.

**Figure 27.** System plot for the  $z = 1.7358$  system towards HE 0515–4411, as described in Fig. 9.

**Figure 28.** System plot for the  $z = 0.7338$  system towards PG 1206+459, as described in Fig. 9.

**Figure 29.** System plot for the  $z = 0.9254$  system towards PG 1206+459, as described in Fig. 9.

**Figure 30.** System plot for the  $z = 0.9276$  system towards PG 1206+459, as described in Fig. 9.

**Figure 31.** System plot for the  $z = 0.9343$  system towards PG 1206+459, as described in Fig. 9.

**Figure 32.** System plot for the  $z = 1.0281$  system towards PG 1206+459, as described in Fig. 9.

**Figure 33.** System plot for the  $z = 0.5507$  system towards PG 1241+176, as described in Fig. 9.

**Figure 34.** System plot for the  $z = 0.5584$  system towards PG 1241+176, as described in Fig. 9.

**Figure 35.** System plot for the  $z = 0.7577$  system towards PG 1241+176, as described in Fig. 9.

**Figure 36.** System plot for the  $z = 0.8954$  system towards PG 1241+176, as described in Fig. 9.

**Figure 37.** System plot for the  $z = 1.2152$  system towards PG 1241+176, as described in Fig. 9.

**Figure 38.** System plot for the  $z = 1.2717$  system towards PG 1241+176, as described in Fig. 9.

**Figure 39.** System plot for the  $z = 0.3946$  system towards PG 1248+401, as described in Fig. 9.

**Figure 40.** System plot for the  $z = 0.5648$  system towards PG 1248+401, as described in Fig. 9.

**Figure 41.** System plot for the  $z = 0.6174$  system towards PG 1248+401, as described in Fig. 9.

**Figure 42.** System plot for the  $z = 0.7011$  system towards PG 1248+401, as described in Fig. 9.

**Figure 43.** System plot for the  $z = 0.7728$  system towards PG 1248+401, as described in Fig. 9.

**Figure 44.** System plot for the  $z = 0.7760$  system towards PG 1248+401, as described in Fig. 9.

**Figure 45.** System plot for the  $z = 0.8545$  system towards PG 1248+401, as described in Fig. 9.

**Figure 46.** System plot for the  $z = 0.6611$  system towards CSO 876, as described in Fig. 9.

**Figure 47.** System plot for the  $z = 0.2854$  system towards PG 1634+706, as described in Fig. 9.

**Figure 48.** System plot for the  $z = 0.6515$  system towards PG 1634+706, as described in Fig. 9.

**Figure 49.** System plot for the  $z = 0.6535$  system towards PG 1634+706, as described in Fig. 9.

**Figure 50.** System plot for the  $z = 0.8182$  system towards PG 1634+706, as described in Fig. 9.

**Figure 51.** System plot for the  $z = 0.9056$  system towards PG 1634+706, as described in Fig. 9.

**Figure 52.** System plot for the  $z = 0.9645$  system towards PG 1634+706, as described in Fig. 9.

**Figure 53.** System plot for the  $z = 0.9904$  system towards PG 1634+706, as described in Fig. 9.

**Figure 54.** System plot for the  $z = 1.0415$  system towards PG 1634+706, as described in Fig. 9.

**Figure 55.** System plot for the  $z = 1.1408$  system towards PG 1634+706, as described in Fig. 9.

**Figure 56.** System plot for the  $z = 1.3413$  system towards PG 1634+706, as described in Fig. 9.

**Figure 57.** System plot for the  $z = 0.7011$  system towards PG 1718+481, as described in Fig. 9.

**Figure 58.** System plot for the  $z = 0.8928$  system towards PG 1718+481, as described in Fig. 9.

**Figure 59.** System plot for the  $z = 1.0065$  system towards PG 1718+481, as described in Fig. 9.

**Figure 60.** System plot for the  $z = 1.0318$  system towards PG 1718+481, as described in Fig. 9.

**Figure 61.** System plot for the  $z = 1.0507$  system towards PG 1718+481, as described in Fig. 9.

**Figure 62.** System plot for the  $z = 1.0548$  system towards PG 1718+481, as described in Fig. 9.

**Figure 63.** System plot for the  $z = 1.0867$  system towards PG 1718+481, as described in Fig. 9.

**Figure 64.** System plot for the  $z = 1.0874$  system towards PG 1718+481, as described in Fig. 9.

This material is available as part of the online article from: <http://www.blackwell-synergy.com/doi/abs/10.1111/j.1365-2966.2007.12097.x>

(This link will take you to the article abstract.)

Please note: Blackwell Publishing are not responsible for the content or functionality of any supplementary materials supplied by the authors. Any queries (other than missing material) should be directed to the corresponding author for the article.

This paper has been typeset from a  $\text{T}_{\text{E}}\text{X}/\text{L}^{\text{A}}\text{T}_{\text{E}}\text{X}$  file prepared by the author.